Kallunki, Juha; Tornikoski, Merja; Björklund, Irene

Identifying 8 mm Radio Brightenings During the Solar Activity Minimum

How much physics is in a current-voltage curve? Inferring defect properties from photovoltaic device measurements

Rachel C. Kurchin, Jeremy R. Poindexter, Ville Vähänissi, Hele Savin, Carlos del Cañizo, Tonio Buonassisi, *Member, IEEE*

Abstract—Defect-assisted recombination processes are critical to understand, as they frequently limit photovoltaic (PV) device performance. However, the physical parameters governing these processes can be extremely challenging to measure, requiring specialized techniques and sample preparation. And yet the fact that they limit performance as measured by current-voltage (JV) characterization indicates that they must have some detectable signal in that measurement. In this work, we use numerical device models that explicitly account for these parameters alongside high-throughput JV measurements and Bayesian inference to construct probability distributions over recombination parameters, showing the ability to recover values consistent with previously-reported literature measurements. The Bayesian approach enables easy incorporation of data and models from other sources; we demonstrate this with temperature dependence of carrier capture cross-sections. The ability to extract these fundamental physical parameters from standardized, automated measurements on completed devices is promising for both established industrial PV technologies and newer research-stage ones.

Index Terms—Bayesian parameter estimation, crystalline silicon, Shockley-Read-Hall (SRH) recombination, high-throughput experiment (HTE), high-performance computing (HPC), iron contamination

I. INTRODUCTION

Recombination mediated by point defects is a performance-limiting mechanism in many photovoltaic (PV) technologies [1–3]. Identifying and characterizing these defects is essential to mitigating their effects. Typically, defect characterization is performed on wafers or semifabricates using temperature- and/or injection-dependent lifetime spectroscopy (TIDLS) [4, 5], deep level transient spectroscopy (DLTS) [6–8], and related spectroscopy techniques. However, these techniques are time-consuming, and the deep expertise necessary to master them is rare. Measurements on semifabricates may not be representative of finished devices, as final processing can affect defect populations. With the maturation of data-science methods, we
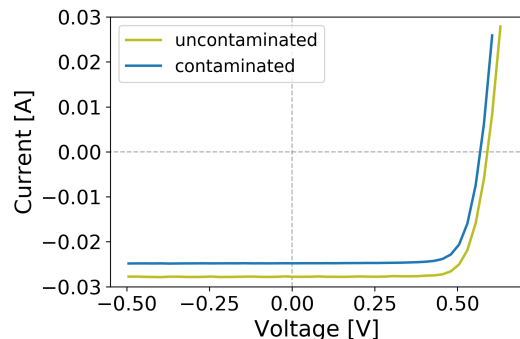
Fig. 1. Current vs. voltage for uncontaminated and intentionally contaminated samples at 300K and 1.01 Sun illumination.

explore the possibility of extracting defect information directly from non-destructive electrical device measurements.

Any defects detrimental to device performance should by definition have a signature in device performance such as current-voltage (JV) measurements. However, such a signal is convoluted with those from so many other physical processes that it cannot be extracted or interpreted through a simple fitting approach, as the fit would be underconstrained. However, by combining current-voltage measurements at a range of temperatures and light intensities ($JVTi$) with physics-based device models [9–11] and Bayesian statistics, these signals can be disentangled, providing fits for many types of underlying parameters, often with greater precision than direct characterization allows.

We previously demonstrated this Bayesian parameter estimation (BPE) approach to measure materials properties such as minority carrier mobility and lifetime in a finished tin sulfide solar cell. [12] The Bayesian framework enables quantifying parameter-specific uncertainty as well as observing emergent relationships between parameters (such as mobility-lifetime product in Reference [12]). In this work, we apply this approach to extract defect-assisted recombination parameters for interstitial iron in silicon, obtaining results consistent with reported literature values. Our results demonstrate a novel approach to extract defect properties from inexpensive measurements of completed devices, demonstrating promise for characterization of both established and novel PV technologies.

II. METHODS

A. Experimental Methods

For this study, silicon solar cells were obtained from the same set used in previous work where samples were intentionally contaminated with specific amounts of interstitial iron (Fe_i); see Ref. [13] ("60A" samples) for details regarding sample fabrication and measurements of iron concentration. Two of these samples were further characterized in this work: one intentionally contaminated sample with a known Fe_i concentration of 2×10^{12} cm^{-3} (after gettering), and a control sample with no intentional contamination (with estimated $[Fe_i] \leq 10^{10}$ cm^{-3}, based on measurement detection limits). Measurements were first performed on a 1-Sun (AM1.5G, 1000W/m^2) solar simulator setup (Newport Oriel Sol3A, class AAA, 450 W Xe lamp, AM1.5G filter, Keithley 2400) to verify open-circuit voltage degradation of less than 1.5% rel. since the samples were first fabricated. Samples were apertured during all JV and $JVTi$ measurements to ensure accurate short-circuit current values would be obtained. QE (PV Measurements QEX7, 300–1100 nm, 75 W Xe lamp, Spectral Products CM110 monochromator) and reflectance data (Perkin-Elmer Lambda 950 UV-Vis spectrophotometer, 150 mm integrating sphere) were also obtained for the purposes of fitting to the PC1D model (see below).

$JVTi$ measurements were performed under vacuum (approx. 10^{-3}–10^{-5} Torr) using a liquid helium cryostat (ARS DE-204SI) and compressor (ARS-4HW) to reach colder sample temperatures while avoiding the condensation of atmospheric species; measurements were taken from 300 to 175 K at increments of 25 K. Precise temperature control within ± 1 K was achieved by placing a thermocouple (Omega CY670) directly on the sample surface and using a polyimide resistive heater (Minco HAP6943) and PID temperature controller (Lakeshore 331) to control total heat flux to the sample. Sample illumination at four different intensities (1.01, 0.69, 0.31, and 0.09 Suns, measured with a silicon photodiode) was achieved using a Newport Oriel Solar Simulator (LCS-100, class ABB, 1.5"×1.5" uniform output) along with an array of neutral-density filters placed within two filter wheels (Thorlabs FW102C). JV sweeps were performed using a Keithley 2400 sourcemeter. To ensure all iron present was in the form of Fe_i (vs. Fe-B pairs), samples were soaked for 15 min at 1 Sun and 300 K before measurements began, as suggested from calculations of temperature-dependent re-pairing rates based on Refs. [14] and [15]. JV data at 300K and 1 Sun illumination are shown in Figure 1. For more JV data and figures of merit (open-circuit voltage, short-circuit current, fill factor), see SI Figures S3 and S4. Diffusion length measurements on a reference wafer performed concurrently with the work in Reference [13] of 140 and 55 μm before and after a light soak, respectively, further support the assertion that Fe_i is the limiting defect. Furthermore, QE measurements (See SI Figure S5) show little difference between samples in the low wavelengths, indicating negligible differences in junction quality.

B. Computational Methods

The 1-Sun JV, quantum efficiency (QE), and reflectance measurements were used to construct a numerical device model accessed by the Bayesian inference framework (see below). The use of a modified, command-line version of PC1D [9, 10] enabled scripted methods for modifying simulation parameters. Specific input parameters were obtained from previous measurements [13], estimated from literature values, or varied in the model to match the JV, QE, and reflectance data of the uncontaminated sample. A full list of device parameters is listed in the Supplementary Information (Tables S1-3).

For the 3-parameter analyses at separate temperatures (shown in Figure 2), BPE was performed on a 3D grid of 36 logarithmically spaced points from 10^{-11} to 10^{-5} s in τ_n, 28 logarithmically spaced points from 10^{-5} to 10^{-1} s in τ_p, and 28 linearly spaced points spanning from the valence band maximum to the conduction band minimum (with energies referenced to the intrinsic Fermi level) in E_t. For the 5-parameter analysis, the grid consisted of 16 logarithmically spaced points from 10^{-19} to 10^{-15} cm^2 in σ_{n0}, 12 logarithmically spaced points from 10^{-16} to 10^{-13} cm^2 in σ_{p0}, 8 linearly spaced points from 0.15 to 0.23 eV in $E_{a,n}$, 9 linearly spaced points from -0.12 to -0.03 eV in $E_{a,p}$, and 16 linearly spaced points from the valence band maximum to 0.16 eV below the conduction band minimum in E_t.

Uniform priors (equal initial probability in every grid box) were used in each analysis; it is worth noting that with hundreds of experimental data points, the final outputs are not very sensitive to the choice of prior. Model uncertainty is estimated from numerical derivatives of model output along the parameter grid, and the standard deviation is taken as the maximum of the model uncertainty and the pre-characterized experimental noise level. We used a modified Gaussian likelihood, wherein the argument was only ever evaluated as an integer number of standard deviations. This has the effect of spreading probability out along grid boxes and reducing incidence of artificially low probability densities arising from the maximally correct parameter space point lying near the edge of a box. This is especially important for the analysis undertaken here, where the output variable can vary extremely sensitively with the input parameters in certain regions of the parameter space.

These BPE calculations were performed using the Bayesim package, for more details see Reference [16], the source code on Github (https://github.com/PV-Lab/bayesim), and/or the package documentation at https://pv-lab.github.io/bayesim/_build/html/index.html. PC1D simulations were run on MIT Supercloud [17] using Wine [18] and the LLMapReduce [19] function. Code to reproduce figures plotted herein is available at https://github.com/PV-Lab/Fe_Si_Bayes_code.

III. THREE-PARAMETER FITS AT SEPARATE TEMPERATURES

Defect-assisted recombination is described by the Shockley-Read-Hall (SRH)[20, 21] equation, where the SRH lifetime
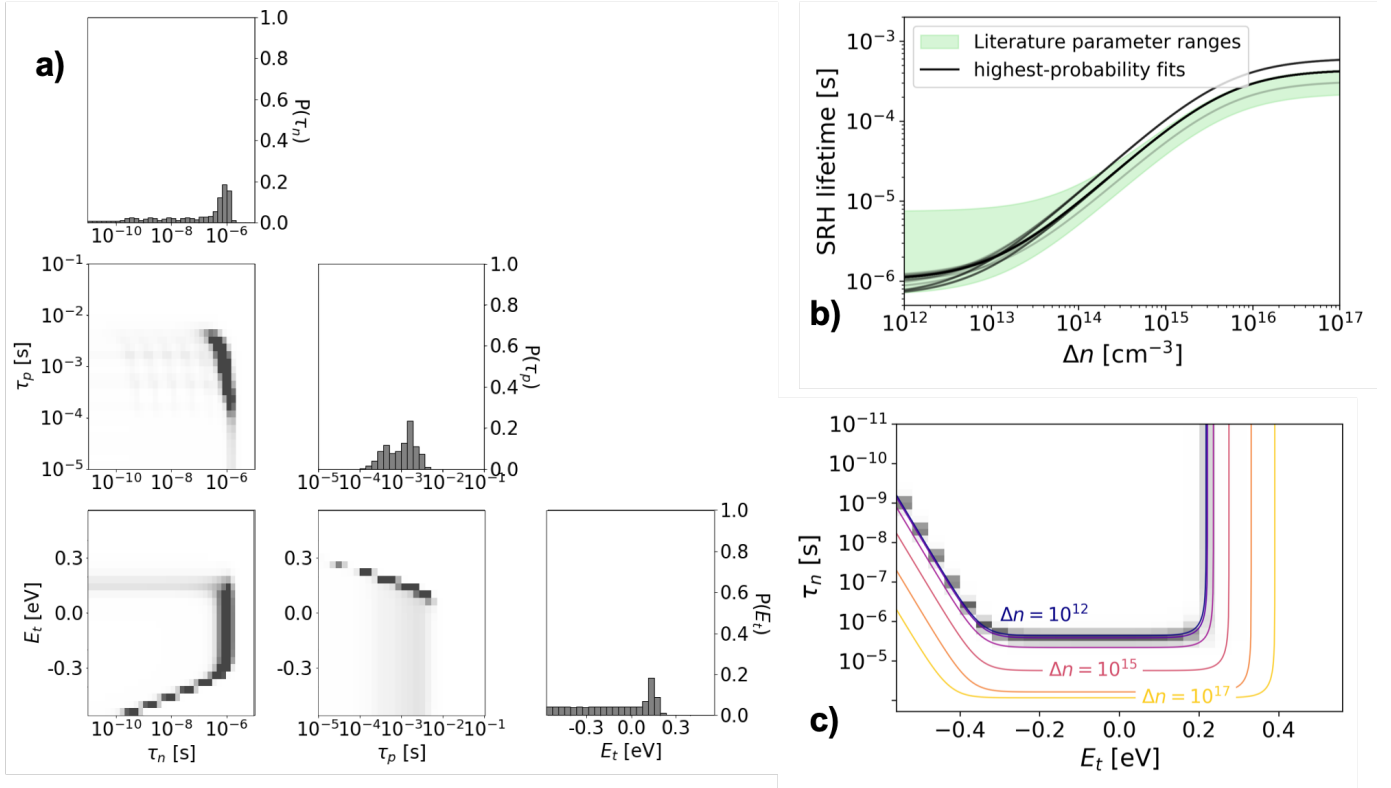
Fig. 2. Visualizations of results of three-parameter fit for contaminated sample at 300K. a) Probability distribution, with single-variable marginalizations along the diagonal and two-variable marginalizations off-diagonal. Two-variable marginalizations have increased contrast relative to defaults (with intensity of color proportional to square root of probability rather than its value) to better show shapes. b) Simulated SRH lifetime vs. injection for the highest probability sets of parameters. Intensity of lines proportional to probability, top 80 parameter sets (corresponding to 46% of total probability mass) shown. Green region shows simulated data based on ranges of parameters found in the literature. c) Marginalization between E_t and τ_n from (a) (but with default visualization contrast) with calculated iso-injection curves overlaid. Each curve differs from the next by a factor of 10.

τ_{SRH} is given by:

$$\tau_{\text{SRH}} = \frac{\tau_n \left(n + n_i \exp\left(\frac{E_t - E_i}{k_B T}\right)\right) + \tau_p \left(p + n_i \exp\left(\frac{E_i - E_t}{k_B T}\right)\right)}{np - n_i^2},$$

(1)

where n, p are the concentrations of electrons and holes, respectively, n_i is the intrinsic electron concentration, E_t is the energy level of the defect (trap), E_i is the intrinsic Fermi level, T is temperature, k_B is Boltzmann's constant, and the lifetime parameters τ_n, τ_p are given by:

$$\tau_n = \frac{1}{N_t \sigma_n v_{\text{th},n}}$$

(2)

$$\tau_p = \frac{1}{N_t \sigma_p v_{\text{th},p}},$$

(3)

where N_t is the defect concentration, σ_n and σ_p are the defect capture cross sections for electrons and holes, respectively, and $v_{\text{th},n}$, $v_{\text{th},p}$ are the thermal velocities of electrons and holes, respectively.

Interstitial iron is one of the most detrimental (and hence best characterized) point defects in silicon PV devices. In this work, we seek to characterize τ_n, τ_p, and E_t from *JVTi* measurements. Varying temperature and illumination intensity is critical to distinguish the influences of different defect parameters. These dependencies on experimental conditions are encoded in PC1D [9, 10], the device simulation software we chose for this study. (For a visualization of the impact of various parameters, see Figure S1) In general, carrier concentrations depend linearly on light intensity. PC1D does not explicitly include temperature dependence of capture cross-sections; we account for this ourselves and the mathematical model is discussed below (see Equations (4) and (5)).

Using *JV* measurements taken from 175–300 K and 0.09–1 Sun, we first construct posterior probability distributions (formally, because they are discrete, probability mass functions, or PMF's) over τ_n, τ_p, and E_t at each temperature separately.(See Methods section for discussion of special likelihood function to capture the correct iso-probability-density curve shapes) An example (at 300 K) is plotted in Figure 2a (See Supplementary Figures S6 and S7 for what this plot would look like with data from only one voltage point and only one illumination level, respectively). Note that, as expected, this PMF does not show a unique high-probability point, as it has been well-established in the literature [4, 22] that without measurements at multiple temperatures and/or doping levels, the SRH equations do not have a unique solution. (We will incorporate data from multiple temperatures into a single fit in the subsequent section, but this simpler analysis can nonetheless be illustrative.)

Next, we choose the highest-probability regions in this

three-dimensional parameter space and use them to construct simulated SRH lifetime curves as a function of carrier injection level, shown in Figure 2b. Also shown (in green) is the range corresponding to the ranges of parameters reported in the literature [4, 23] and constructed using tabulated values for thermal velocities in silicon [24] and previously-characterized defect densities on this sample [13]. The simulated curves from this study are generally within the literature ranges (see discussion below regarding disagreement at high injection).

Figure 2c shows the marginal distribution between τ_n and E_t from Figure 2a, with iso-injection curves overlaid. These were constructed using a fixed τ_p value for the purposes of visualization, chosen as roughly the center (i.e. logarithmic average) of the high-density region in Figure 2a. τ_{SRH} was fixed to the logarithmic average over the range computed from literature parameters in Figure 2b, and then Equation (1) inverted to give a relationship between τ_n and E_t. The results are consistent with the fact that these devices should be in low injection under the illumination levels used. (Interestingly, in Figure 2b we also see a better agreement with literature in low injection, emphasizing the importance of data spanning all relevant conditions to get the best fit.) This analysis again demonstrates that similar information to lifetime spectroscopy can be gleaned from our approach.

IV. FIVE-PARAMETER FIT ACROSS ALL TEMPERATURES

As alluded to above, because thermal velocities in silicon are tabulated and trap density in this sample has been characterized, we can directly correspond time constants to capture cross sections (see Equations (2) and (3)). A widely-accepted model for carrier capture is as a thermally activated process [23, 25] Implementing such a model allows an Arrhenius relation to be used for each capture cross-section, introducing two new parameters for each carrier: a prefactor σ_0 and an activation energy E_a:

$$\sigma_n = \sigma_{n0}e^{E_{a,n}/k_B T} \tag{4}$$

$$\sigma_p = \sigma_{p0}e^{E_{a,p}/k_B T}. \tag{5}$$

The parameter space is now five-dimensional, but we can also constrain a single posterior distribution using all the data rather than needing separate fits at each temperature. The probability distribution resulting from this analysis is shown in Figure S2. Moving forward, we focus on σ_p in literature data comparisons, because significantly more data has been reported than for σ_n. Figure 3a shows an excerpt from Figure S2, namely, the marginalization between $E_{a,p}$ and σ_{p0}. The line of similar posterior probability seen in Figure 3a (note that σ_{p0} is logarithmically spaced) represents the inherent tradeoff between prefactor and activation energy when fitting an exponential model like this over a finite temperature range. This tradeoff is clear from Figure 3b, which shows the literature-sourced σ_p values at discrete temperatures as well as the lines corresponding to the highest-probability Arrhenius parameter sets from this analysis. See SI Figure S3 for comparisons between modeled and observed JV data at all sets of experimental conditions. Literature values are
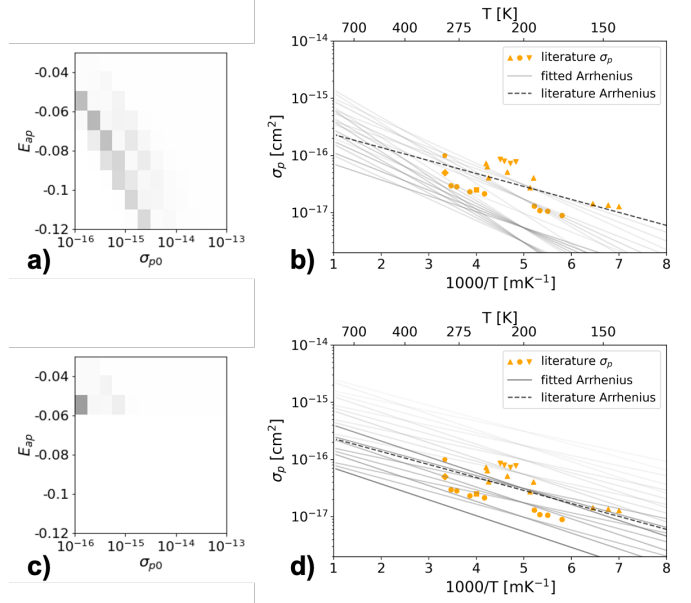

Fig. 3. a) $E_{a,p}$-σ_{p0} marginalization from five-parameter Arrhenius fit. (Excerpt from Figure S2) b) σ_p data from literature (References 23, 26–32) with inferred Arrhenius fits, intensity of line proportional to probability of parameters, and Arrhenius fit from literature [23]. c) Marginalization from (a) conditioned on $E_{a,p}$ value being within .01 eV of the literature value of -0.045 eV. d) Same plot as (b) but for the marginalized PMF from (c). (top 20 Arrhenius fit parameter sets plotted in both (b) and (d))

from Refs. [26–32] and were originally collated by Ref. [23]; acquisition methods include DLTS, thermally stimulated capacitance (TSCAP, a predecessor technique to DLTS), and Hall effect.

The dotted line in Figure 3b represents the Arrhenius fit from Ref. [23]. However, that fit allowed only the prefactor to vary, fixing the activation energy according to the results of a separate measurement, while in our analysis we allowed the activation energy to be a fitting parameter. A strength of the Bayesian approach is that information from such a measurement can be explicitly incorporated via conditioning the posterior distribution further. To do this, we simply set the probability to zero in all grid boxes that do not have activation energies near this value (-0.045 eV), then renormalize the overall distribution. After this operation, Figure 3a becomes Figure 3c, and 3b becomes 3d, with the results agreeing even more closely with the literature fit.

V. CONCLUSIONS

In this work, we demonstrate the ability to extract SRH recombination parameters from device-level measurements (rather than characterization of semifabricates) and Bayesian parameter estimation utilizing a modified Gaussian likliehood that yields comparable results to TIDLS and DLTS. In particular, our results fall well within the range of values reported by different DLTS practitioners, and simulated IDLS data are also in agreement. However, our approach utilizes a much simpler and more widely applicable experimental setup – a temperature-controlled JV stage with a solar simulator and neutral-density filters, making defect characterization potentially accessible to a broader range of researchers, including

those investigating earlier-stage materials. Furthermore, *JV* measurement is a standard industrial characterization technique, meaning this approach could be integrated into manufacturing environments where samples from production lines could be tested using this technique to provide valuable feedback into impurities introduced during the manufacturing process, potentially utilizing sample heating rather than (or in addition to) cooling to remove the need for a cryostat. It also shifts a significant number of person-hours of effort to computational resources, which are becoming increasingly inexpensive, plentiful, and user-friendly. In addition, the Bayesian framework allows easy incorporation of any preexisting information from other sources, such as (in this work) parametrization of thermal velocity or prior characterization of trap density or capture barrier. We note that within the range of experimental conditions of our measurements (in particular, all measurements being in the low-injection regime), we were not able to significantly constrain the trap level. This would likely be resolved with a setup capable of concentrated measurements significantly above 1 Sun of illumination. Another interesting direction in this regard would be applying the BPE approach to Suns-V_{oc} measurements.

In this study, we investigated a system (interstitial iron) for which parameters have been extensively reported in the literature to allow for validation of results. We believe that this approach could be used for identification of unknown defects provided that there is reasonable confidence of one defect dominating the SRH signal (a frequent but not universal occurrence). However, if multiple defects were present, it is likely that some prior knowledge constraining their parameters relative to each other would be needed, as it has been shown that unambiguous identification of two defects is not feasible in all cases. [33]

We emphasize that in any analysis of this kind, the quality of the results obtained is strictly bounded above by the applicability of the model whose parameters are being estimated. For example, if in reality the temperature dependence of capture cross sections deviates from a thermally activated model, the meaning of the associated parameters and their probability distributions could be called into doubt as well. (Some authors [34, 35] have also suggested a power law relationship between capture cross section and temperature.)

This work represents a simple, rapid ($\mathcal{O}(1$ day$)$ each experiment time and simulation time on a sufficient HPC cluster) approach to access SRH parameters from finished devices, which promises to be useful both in screening of novel PV materials as well as characterizing better-known ones, as defect parameter data is generally very sparse in literature due to the complexity of its collection.

REFERENCES

[1] M. Schubert, M. Padilla, B. Michl, L. Mundt, J. Giesecke, J. Hohl-Ebinger, J. Benick, W. Warta, M. Tajima, and A. Ogura, "Iron related solar cell instability: Imaging analysis and impact on cell performance," *Solar Energy Materials and Solar Cells*, vol. 138, pp. 96–101, 2015. [Online]. Available: https://linkinghub.elsevier.com/retrieve/pii/S0927024815001026

[2] A. Collord, H. Xin, and H. W. Hillhouse, "Combinatorial exploration of the effects of intrinsic and extrinsic defects in $Cu_2ZnSn(S,Se)_4$," *IEEE Transactions on Electron Devices*, vol. 5, no. 1, pp. 288–298, 2015. [Online]. Available: http://ieeexplore.ieee.org/xpls/abs_all.jsp?arnumber=6945352

[3] K. Durose, "High efficiency for As-doped cells," *Nature Energy*, vol. 4, no. 10, pp. 825–826, 2019. [Online]. Available: http://www.nature.com/articles/s41560-019-0475-2

[4] S. Rein, T. Rehrl, W. Warta, and S. W. Glunz, "Lifetime spectroscopy for defect characterization: Systematic analysis of the possibilities and restrictions," *Journal of Applied Physics*, vol. 91, no. 3, pp. 2059–2070, 2002.

[5] A. E. Morishige, M. A. Jensen, D. B. Needleman, K. Nakayashiki, J. Hofstetter, T. T. A. Li, and T. Buonassisi, "Lifetime spectroscopy investigation of light-induced degradation in p-type multicrystalline silicon PERC," *2017 IEEE 44th Photovoltaic Specialist Conference, PVSC 2017*, vol. 6, no. 6, pp. 1–7, 2017.

[6] D. V. Lang, "Deep-level transient spectroscopy: A new method to characterize traps in semiconductors," *Journal of Applied Physics*, vol. 45, no. 7, p. 3023, 1974. [Online]. Available: http://scitation.aip.org/content/aip/journal/jap/45/7/10.1063/1.1663719

[7] N. M. Johnson, "Deep level transient spectroscopy: Defect characterization in semiconductor devices," *MRS Proceedings*, vol. 69, pp. 75–94, 1986.

[8] D. Wickramaratne, C. E. Dreyer, B. Monserrat, J. X. Shen, J. L. Lyons, A. Alkauskas, and C. G. Van de Walle, "Defect identification based on first-principles calculations for deep level transient spectroscopy," *Applied Physics Letters*, vol. 113, no. 19, 2018.

[9] H. Haug, J. Greulich, A. Kimmerle, and E. S. Marstein, "PC1Dmod 6.1 – state-of-the-art models in a well-known interface for improved simulation of Si solar

cells," *Solar Energy Materials and Solar Cells*, vol. 142, pp. 47–53, 2015. [Online]. Available: https://linkinghub.elsevier.com/retrieve/pii/S0927024815002640

[10] H. Haug and J. Greulich, "PC1Dmod 6 . 2 – Improved simulation of c-Si devices with updates on device physics and user interface," *Energy Procedia*, vol. 92, no. 1876, pp. 60–68, 2016. [Online]. Available: http://dx.doi.org/10.1016/j.egypro.2016.07.010

[11] M. Burgelman, P. Nollet, and S. Degrave, "Modelling polycrystalline semiconductor solar cells," *Thin Solid Films*, vol. 361-362, pp. 527–532, 2000. [Online]. Available: http://www.sciencedirect.com/science/article/pii/S0040609099008251

[12] R. E. Brandt, R. C. Kurchin, V. Steinmann, D. Kitchaev, C. Roat, S. Levcenco, G. Ceder, T. Unold, T. Buonassisi, and H. Z. Berlin, "Rapid semiconductor device characterization through Bayesian parameter estimation," *Joule*, vol. 1, no. 4, pp. 843–856, 2017. [Online]. Available: https://doi.org/10.1016/j.joule.2017.10.001

[13] V. Vähänissi, A. Haarahiltunen, H. Talvitie, M. Yli-koski, and H. Savin, "Impact of phosphorus gettering parameters and initial iron level on silicon solar cell properties," *Progress in Photovoltaics: Reseach and Applications*, pp. 1127–1135, 2013.

[14] D. Macdonald, T. Roth, P. N. K. Deenapanray, T. Trupke, and R. A. Bardos, "Doping dependence of the carrier lifetime crossover point upon dissociation of iron-boron pairs in crystalline silicon," *Applied Physics Letters*, vol. 89, no. 14, p. 142107, 2006. [Online]. Available: http://aip.scitation.org/doi/10.1063/1.2358126

[15] G. Zoth and W. Bergholz, "A fast, preparation-free method to detect iron in silicon," *Journal of Applied Physics*, vol. 67, no. 11, pp. 6764–6771, 1990. [Online]. Available: http://aip.scitation.org/doi/10.1063/1.345063

[16] R. Kurchin, G. Romano, and T. Buonassisi, "Bayesim: A tool for adaptive grid model fitting with Bayesian inference," *Computer Physics Communications*, vol. 239, pp. 161–165, 2019. [Online]. Available: https://doi.org/10.1016/j.cpc.2019.01.022

[17] A. Reuther, J. Kepner, C. Byun, S. Samsi, W. Arcand, D. Bestor, B. Bergeron, V. Gadepally, M. Houle, M. Hubbell, M. Jones, A. Klein, L. Milechin, J. Mullen, A. Prout, A. Rosa, C. Yee, and P. Michaleas, "Interactive Supercomputing on 40,000 Cores for Machine Learning and Data Analysis," in *2018 IEEE High Performance Extreme Computing Conference (HPEC)*. IEEE, 2018, pp. 1–6. [Online]. Available: https://ieeexplore.ieee.org/document/8547629/

[18] "Wine." [Online]. Available: https://www.winehq.org

[19] C. Byun, J. Kepner, W. Arcand, D. Bestor, B. Bergeron, V. Gadepally, M. Hubbell, P. Michaleas, J. Mullen, A. Prout, A. Rosa, C. Yee, and A. Reuther, "LLMapReduce: Multi-level map-reduce for high performance data analysis," in *2016 IEEE High Performance Extreme Computing Conference (HPEC)*. IEEE, 2016, pp. 1–8. [Online]. Available: http://ieeexplore.ieee.org/document/7761618/

[20] W. Shockley and W. T. Read, "Statistics of the recombi-nation of holes and electrons," *Physical Review*, vol. 87, no. 46, pp. 835–842, 1952.

[21] R. N. Hall, "Electron-hole recombination in germanium," *Physical Review*, vol. 87, no. 2, p. 387, 1952.

[22] J. D. Murphy, K. Bothe, R. Krain, V. Voronkov, and R. Falster, "Parameterisation of injection-dependent lifetime measurements in semiconductors in terms of shockley-read-hall statistics: An application to oxide pre-cipitates in silicon," *Journal of Applied Physics*, vol. 111, no. 11, p. 113709, 2012.

[23] A. A. Istratov, H. Hieslmair, and E. R. Weber, "Iron and its complexes in silicon," *Applied Physics A*, vol. 44, pp. 13–44, 1999. [Online]. Available: https://doi.org/10.1007/s003390050968

[24] M. A. Green, "Intrinsic concentration, effective densities of states, and effective mass in silicon," *Journal of Applied Physics*, vol. 67, no. 6, pp. 2944–2954, 1990.

[25] R. Pässler, "Temperature dependences of the nonradiative multiphonon carrier capture and ejection properties of deep traps in semiconductors. I. Theoretical results," *Physica Status Solidi (b)*, vol. 85, no. 1, pp. 203–215, 1978. [Online]. Available: http://doi.wiley.com/10.1002/pssb.2220850122

[26] H. Lemke, "Dotierungseigenschaften von Eisen in Silizium," *Physica Status Solidi (a)*, vol. 64, no. 1, pp. 215–224, 1981. [Online]. Available: http://doi.wiley.com/10.1002/pssa.2210640123

[27] ——, "Zum Nachweis von Rekombinationszentren in den Basiszonen von Si-Gleichrichtern," *Physica Status Solidi (a)*, vol. 63, no. 1, pp. 127–136, 1981. [Online]. Available: http://doi.wiley.com/10.1002/pssa.2210630117

[28] K. Wünstel and P. Wagner, "Interstitial iron and iron-acceptor pairs in silicon," *Applied Physics A Solids and Surfaces*, vol. 27, no. 4, pp. 207–212, 1982. [Online]. Available: http://link.springer.com/10.1007/BF00619081

[29] S. D. Brotherton, P. Bradley, and A. Gill, "Iron and the iron-boron complex in silicon," *Journal of Applied Physics*, vol. 57, no. 6, pp. 1941–1943, 1985. [Online]. Available: http://aip.scitation.org/doi/10.1063/1.335468

[30] H. Indusekhar and V. Kumar, "Properties of iron related quenched-in levels in p-silicon," *physica status solidi (a)*, vol. 95, no. 1, pp. 269–278, 1986. [Online]. Available: http://doi.wiley.com/10.1002/pssa.2210950134

[31] X. Gao, H. Mollenkopf, and S. Yee, "Annealing and profile of interstitial iron in boron-doped silicon," *Applied Physics Letters*, vol. 59, no. 17, pp. 2133–2135, 1991. [Online]. Available: http://aip.scitation.org/doi/10.1063/1.106103

[32] S. Rein and S. W. Glunz, "Electronic properties of interstitial iron and iron-boron pairs determined by means of advanced lifetime spectroscopy," *Journal of Applied Physics*, vol. 98, no. 11, 2005.

[33] T. U. Narland, S. Bernardini, M. S. Wiig, and M. I. Bertoni, "Is it possible to unambiguously assess the presence of two defects by temperature- and injection-dependent lifetime spectroscopy?" *IEEE Journal of Photovoltaics*, vol. 8, no. 2, pp. 465–472, 2018.

[34] B. B. Paudyal, K. R. McIntosh, and D. H. Macdonald, "Temperature dependent electron and hole capture cross sections of iron-contaminated boron-doped silicon," in *2009 34th IEEE Photovoltaic Specialists Conference (PVSC)*, June 2009, pp. 001 588–001 593.

[35] K. Graff, *Metal Impurities in Silicon-Device Fabrication*, ser. Springer Series in Materials Science. Springer-Verlag, 1995, no. 24.

Carlos del Cañizo is a Full Professor at Universidad Politécnica de Madrid and director of its Solar Energy Institute. He has been involved in Photovoltaic research for more than 25 years, working on the manufacturing and characterisation of solar cells, on defect engineering techniques in silicon, and also in the field of silicon refinement.

Rachel C. Kurchin received a PhD in Materials Science and Engineering from the Massachusetts Institute of Technology, Cambridge, MA, USA in 2019, an MPhil in Materials Science & Metallurgy from the University of Cambridge, Cambridge, UK, in 2014, and a B.S. degree in Physics (Intensive) from Yale University, New Haven, CT, USA in 2013.

She is currently a postdoctoral fellow at Carnegie Mellon University in Pittsburgh, PA, USA working on data science and machine learning for the optimization of fuel cells and next-generation lithium-ion batteries.

Jeremy R. Poindexter received a Ph.D. degree in Materials Science and Engineering from the Massachusetts Institute of Technology, Cambridge, MA, USA in 2018 and a B.S. degree in Mechanical Engineering from Yale University, New Haven, CT, USA in 2011. His research has focused on performance-limiting mechanisms due to point defects in early-stage photovoltaic materials, as well as various opto-electronic characterization techniques such as time-resolved photoluminescence and quantum efficiency. He currently works as a Senior Process Development Engineer for Tesla.

Tonio Buonassisi (M'13) received his Ph.D. in Applied Science and Technology from the University of California at Berkeley, Berkeley, CA, USA, in 2006, with additional research with the Fraunhofer Institute for Solar Energy Systems, Freiburg, Germany, and the Max-Planck-Institute for Microstructure Physics, Halle, Germany. He is currently the Head of the Photovoltaic Research Laboratory, Massachusetts Institute of Technology, Cambridge, MA, USA, which combines machine learning, high-throughput experiments, and high-performance computing to accelerate the development of energy-relevant materials and systems. Thematic areas include processing, characterization, defects, and cost-performance modeling to engineer naturally abundant and manufacturable materials into cost-effective high-performance devices.

Ville Vähänissi received the D.Sc. (Tech.) degree in semiconductor technology in 2016 from Aalto University, Helsinki, Finland. His research interests include defect engineering in silicon, especially photovoltaics, as well as atomic layer deposition and its various applications in semiconductor devices.

He is currently working as a Staff Scientist at the Department of Electronics and Nanoengineering at Aalto University School of Electrical Engineering.

Hele Savin received the D.Sc. (Tech.) degree in semiconductor technology in 2005 from Aalto University, Finland. Her research interests focus on material research in semiconductors, more specifically defect engineering in silicon, nanostructured silicon, light-induced degradation and silicon photodetectors.

She is currently an Associate Professor in the Department of Electronics and Nanoengineering, Aalto University, Finland.